BIOCHEMISTRY
including biophysical chemistry & molecular biology
Article

Biochemistry **2009,** *48,* 10321–10333 10321
DOI: 10.1021/bi901115z

Mutual Exchange of Kinetic Properties by Extended Mutagenesis in Two Short LOV Domain Proteins from *Pseudomonas putida*†

Katrin Jentzsch,‡ Astrid Wirtz,‡ Franco Circolone,‡ Thomas Drepper,‡ Aba Losi,§ Wolfgang Gärtner,∥ Karl-Erich Jaeger,‡ and Ulrich Krauss*,‡

‡*Institut für Molekulare Enzymtechnologie, Heinrich-Heine Universität Düsseldorf, FZ-Jülich, Stetternicher Forst D-52426 Jülich, Germany,* §*Department of Physics, University of Parma, Parma, Italy, and* ∥*Max-Planck-Institute for Bioinorganic Chemistry, Mülheim, Germany*

Received July 1, 2009; Revised Manuscript Received September 21, 2009

ABSTRACT: We previously characterized a LOV protein PpSB2-LOV, present in the common soil bacterium *Pseudomonas putida*, that exhibits a plant phototropin LOV-like photochemistry [Krauss, U., Losi, A., Gärtner, W., Jaeger, K. E., and Eggert, T. (2005) *Phys. Chem. Chem. Phys. 7*, 2804−2811]. Now, we have identified a second LOV homologue, PpSB1-LOV, found in the same organism with approximately 66% identical amino acids. Both proteins consist of a conserved LOV core flanked by short N- and C-terminal extensions but lack a fused effector domain. Although both proteins are highly similar in sequence, they display drastically different dark recovery kinetics. At 20 °C, PpSB2-LOV reverts with an average time constant of 137 s from the photoequilibrium to the dark state, whereas PpSB1-LOV exhibits an average dark recovery time constant of 1.48×10^5 s. Irrespective of the significant differences in their dark recovery behavior, both proteins showed nearly identical kinetics for the photochemically induced adduct formation. In order to elucidate the structural and mechanistic basis of these extremely different dark recovery time constants, we performed a mutational analysis. Six amino acids in a distance of up to 6 Å from the flavin chromophore, which differ between the two proteins, were identified and interchanged by site-directed mutagenesis. The amino acid substitution R66I located near the FMN phosphate in LOV domains was identified in PpSB1-LOV to accelerate the dark recovery by 2 orders of magnitude. *Vice versa*, the corresponding substitution I66R slowed down the dark recovery in PpSB2-LOV by a factor of 10. Interestingly, the interchange of the C-terminal extensions between the two proteins also had a pronounced effect on the dark recovery time constants, thus highlighting a coupling of these protein regions to the chromophore binding pocket.

Many organisms depend on the ability to sense the quality and quantity of the incoming radiation in order to optimally respond to changing light environments by optimizing the yield of photosynthesis, fine-tuning their metabolism to environmental/nutritional conditions, or avoiding harmful irradiation. Detection of physical parameters, such as wavelength distribution or intensity and duration of light exposure, needs to be integrated in order to produce a balanced physiological response. One class of photoreceptor sensor modules are the so-called light, oxygen, voltage (LOV)[1] domains (*1*). LOV domains show an absorption in the blue spectral region due to a noncovalently bound flavin chromophore (FMN (flavin mononucleotide), λ_{max} around 447 nm). They were initially identified as the light-sensing part of plant phototropins (phot), the primary blue light photoreceptors for plant phototropism (*2*), chloroplast movement, leaf expansion, and stomata opening (*3*).

In the past decade, genome mining revealed that LOV signaling modules are equally widespread in the prokaryotic world (*4*). The first prokaryotic LOV domain-containing protein that was biochemically and biophysically characterized was YtvA from *Bacillus subtilis* (*5*). Subsequently, LOV domain homologous sequences were identified in a variety of phototrophic and chemotrophic prokaryotes. Consequently, biochemical studies on various prokaryotic LOV proteins were conducted and revealed that the LOV-signaling paradigm is conserved between eu- and prokaryotes (*5*−*7*). Studies on light-dependent physiological effects in prokaryotes are still sparse; a regulation of the general stress response, cell−cell attachment, and the regulation of virulence have been reported so far (*8*−*10*).

Despite their origin from pro- or eukaryotic organisms, the photochemistry and the following (thermally) driven reactions of LOV domains are principally the same and differ mainly in the kinetic time constants for the respective reactions. Absorption of light by the protein in the dark state, that maximally absorbs at 447 nm (LOV447), generates the singlet excited state of FMN that undergoes on a nanosecond time scale an intersystem crossing process to form the corresponding triplet state, that shows a red-shifted absorption maximum at 660 nm (LOV660) (*11*). In turn, LOV660 decays within a few microseconds to give rise to a covalent adduct between the C4a carbon atom of the flavin isoalloxazine ring and the thiol group of a closely positioned cysteine residue, which results in a shift of the absorption maximum to 390 nm (LOV390). This blue-shifted absorbing species is considered the signaling state of LOV domains (*12*−*14*). Although the nature of the distinguishable

†This work was supported by the Deutsche Forschungsgemeinschaft (Forschergruppe FOR526).

*Corresponding author: phone, ++492461612939; fax, ++492461612490; e-mail, u.krauss@fz-juelich.de.

[1]Abbreviations: LOV, light, oxygen, voltage; FMN, flavin mononucleotide; phot, phototropin; FKF1, flavin-binding Kelch-repeat F-box protein 1.

Published on Web 09/22/2009

intermediates of the LOV photocycle is well established, the exact mechanism by which the covalent bond is formed is yet under discussion. In brief, two reaction mechanisms for covalent adduct formation have been suggested: (i) an ionic model and (ii) a radical pair mechanism (*15*). Recent FT-IR studies (*16*, *17*) as well as theoretical (quantum mechanical) considerations (*18*, *19*) disfavor an ionic mechanism but, however, cannot rule it out completely (*16*). In the dark, the covalent bond formation is reversible, whereas the bond reopens within minutes or hours for various LOV proteins (*5*, *6*, *20*−*22*). For some proteins, e.g., the flavin-binding Kelch-repeat F-box protein (FKF1) of *Arabidopsis*, the recovery can take up to several days (*21*). While the primary events in the LOV photocycle are mechanistically relatively well understood, the molecular basis of the dark recovery kinetics is far from being resolved.

Early on, the dark recovery of plant phototropin LOV domains was suggested to be base-catalyzed due to an observed pH dependence of the process with a suggested p*K* value between 5 and 6 (*12*, *13*). However, no basic amino acids are found in close proximity to the FMN chromophore in the different available plant LOV domain structures (*23*, *24*). Therefore, it was speculated that general base catalysis occurs from surface-exposed histidine residues located distantly from the FMN chromophore via a network formed by the base, the chromophore, and intraprotein water molecules (*13*). This suggestion recently found support in a study by Alexandre and co-workers that demonstrated (i) that imidazole can act as an efficient enhancer of the dark recovery rate and (ii) that blocking of histidines by diethyl pyrocarbonate slows down the recovery (*25*).

In a detailed study, Christie and co-workers employed a random mutagenesis approach to identify residues in the LOV2 domain of *Avena sativa* phot1 (As-phot1 LOV2), which influence the dark recovery kinetics and the LOV photochemistry. They identified one amino acid residue (I427, As-phot1 numbering) with an outstanding functional effect in van der Waals contact with the sulfur atom of the photoreactive cysteine residue that upon exchange to valine accelerated the dark recovery 10-fold. The authors thus concluded that steric interactions in the protein around the FMN chromophore can influence the dark recovery process (*26*). Moreover, LOV1−LOV2 tandem constructs showed altered dark recovery rates, implying that protein−protein interactions also contribute to the process (*27*).

We recently reported the photochemical and biochemical characterization of a LOV blue light signaling module (termed PpSB2-LOV) (*6*), identified in the plant-root colonizing proteobacterium *Pseudonomas putida* KT2440. Here we present evidence that the same microorganism possesses a second LOV protein (termed PpSB1-LOV) that is highly conserved in sequence to PpSB2-LOV (66% identical amino acid positions) but displays significantly different photochemical behavior with respect to dark state recovery kinetics. The respective dark recovery time constants observed for the two proteins differ by 3 orders of magnitude, being much faster for PpSB2-LOV. Both proteins consist of a conserved LOV core flanked by N- and C-terminal extensions but lack a fused effector domain.

The mechanistic and structural reasons for these drastically different dark recovery kinetics were studied by an extensive mutational analysis. Several amino acids that are localized in close proximity to the FMN chromophore and differ between the two proteins were interchanged. Furthermore, we interchanged the C-terminal, putatively helical extension between the two proteins. Using this approach we have identified one amino acid position, located in close proximity to the FMN phosphate on helix Fα that is a major determinant for the velocity of the photocycle. Remarkably, the interchange of the C-terminal extension had a pronounced effect on the dark recovery. Besides influencing the kinetics of the dark recovery process, a change in selectivity of the incorporated chromophore was caused by the mutation.

MATERIALS AND METHODS

Bacterial Strains and Plasmids. All bacterial strains used in this study were grown either in Luria−Bertani (LB) broth or in autoinduction (AI) media (adapted from ref *28*) for heterologous expression of recombinant proteins. In brief, the media consisted of 12 g/L casein hydrolysate, 24 g/L yeast extract, and 5 g/L glycerol, in 100 mM potassium phosphate buffer, pH 7.0. The media were supplemented for induction with 0.5 g/L glucose and 2 g/L lactose, respectively. The genes coding for the two LOV proteins, PpSB1-LOV (Swiss Prot: Q88E39) and PpSB2-LOV (Swiss Prot: Q88JB0), were cloned in a similar manner as described previously for PpSB2-LOV (*6*). In this study, we used a construct of PpSB2-LOV that, in contrast to the formerly described one (*6*), lacks the first three N-terminal amino acids. All constructs were expressed as N-terminal hexahistidine tagged fusion proteins (tag sequence: MGSSHHHHHHSSGLVPRGSH) in *Escherichia coli* BL21(DE3). Overexpression was carried out either in 50 mL cultures (for the prescreening) or in 1 L AI media cultures for 3 h at 37 °C after which the cultures were shifted to 30 °C. Subsequently, the cells were incubated for 48 h (prescreening) or 72 h (large-scale overexpression) at constant agitation (120 rpm) in the dark.

General Molecular Biological Techniques. Isolation of recombinant plasmids, gel extraction of DNA fragments, DNA ligation, and transformation into *E. coli* strains were carried out according to standard laboratory protocols (*29*).

Site-Directed Mutagenesis and Construction of Variants. The genes encoding full-length PpSB1-LOV and PpSB2-LOV in pET28a were used as template DNA for PCR mutagenesis. Site-directed mutagenesis was carried out using the QuikChange mutagenesis technique according to the instructions given by the manufacturer (Stratagene, La Jolla, CA). In most cases, Turbo-*Pfu* DNA polymerase (Stratagene) was used for amplification. The oligonucleotide primer sequences used throughout this study are summarized in Supporting Information Table 1.

Overall, six point mutations were introduced into each protein. The mutations introduced into PpSB1-LOV were A13H, K23Q, E47D, R61H, R66I, and K71E. Correspondingly, the mutations generated for PpSB2-LOV were H13A, Q23K, D47E, H61R, I66R, and E71K.

In order to generate mutants with interchanged C-terminal extensions, we introduced a *Zra*I restriction site by QuikChange mutagenesis into the PpSB2-LOV gene at the immediate end of the LOV core domain (following D118 in the translated PpSB2-LOV core gene). PpSB1-LOV already possesses a *Zra*I site at the respective position in the gene. This allowed for the straightforward interchange of the C-terminal extensions between PpSB1-LOV and the PpSB2-LOV mutant with the introduced *Zra*I site by subcloning. All generated mutants were verified by sequencing.

Small-Scale Prescreening of PpSB1-LOV and PpSB2-LOV Variants. After overexpression in small scale (see above),

the cultures were harvested by centrifugation for 30 min at 5000 rpm at 4 °C. The resulting cell pellet was resuspended in 5 mL of 10 mM sodium phosphate buffer (pH 8.0) supplemented with 10 mM NaCl. Cells were broken by sonication for 2 min on ice. The procedure was repeated four to five times until complete cell lysis was observed. Cell debris and unbroken cells were removed by centrifugation for 10 min at 14000 rpm at 4 °C. The crude cell extract was transferred into fresh Eppendorf tubes and stored in the dark at 4 °C until further processing.

A first evaluation of the kinetic behavior of the generated PpSB1-LOV and PpSB2-LOV variants was achieved using crude cell extracts (prepared as described above) in a microtiter plate (MTP) based prescreening approach. In brief, the respective dark recovery kinetics were measured by recording a kinetic trace at 480 nm absorbance after illumination of all samples in the MTP wells for 30 s using a custom-made 96-well LED illuminator (Fa. Seltsam, Aachen, Germany). All measurements were performed using a SpectraMax 250 MTP photometer (Molecular Devices, Ramsey, MN) thermostated to 30 °C. Each MTP well contained 150 μL of cell crude cell extracts of the respective overexpressing strain. For each variant the kinetic measurement was performed in triplicate. A 10 mM sodium phosphate buffer (pH 8.0) supplemented with 10 mM NaCl was used as reference. Crude cell extracts from a strain harboring only the empty pET28a plasmid and the crude cell extracts of cultures expressing the respective wild-type PpSB1-LOV and PpSB2-LOV proteins were used as controls.

Large-Scale Protein Overexpression and Purification. The wild-type and selected mutant LOV proteins were expressed in large scale as described above and purified using immobilized metal affinity chromatropgraphy (IMAC) as described previously (*6*). After elution from the IMAC column, the pooled LOV protein containing fractions were desalted using a VivaSpin concentrator unit (10 kDa MWCO). The final buffer was 10 mM sodium phosphate buffer (pH 8.0) supplemented with 10 mM of NaCl. All purified proteins were stored at 4 °C in the dark until further use.

Spectroscopic Techniques. All spectroscopic work was carried out under dim red safety light. Measurement of the light-dependent absorption changes in the UV/vis region (200−600 nm) was carried out using a UV-2401PC UV/vis spectrophotometer with temperature control set to 20 °C (Shimadzu, Duisburg, Germany). Protein samples were diluted in 10 mM sodium phosphate buffer supplemented with 10 mM NaCl (pH 8.0) to a final absorbance at 450 nm of about 0.2. The same buffer was used as a reference. After recording of the protein dark state spectra, the samples were illuminated for 30 s using a blue light emitting Led-Lensers V8 lamp (Zweibrüder Optoelectronics, Solingen, Germany). Subsequently, the light state spectrum was recorded.

The dark state recovery was measured from illuminated samples by recording the absorption recovery at 480 nm for 1.5 h in the case of the PpSB2-LOV variants and over a total time period of 30 h for PpSB1-LOV, respectively. All measurements were carried out at 20 °C. All recovery kinetics of PpSB2-LOV variants were measured at least three times for two independent protein preparations. Due to the very slow recovery of the PpSB1-LOV proteins, the samples were only measured twice for two independent protein preparations of each variant and wild-type protein.

Tryptophan fluorescence spectra for the proteins in their dark-adapted state were recorded as described previously (*6*). Circular dichroism (CD) spectra were accumulated for all mutant and wild-type proteins using a JASCO J-810 spectropolarimeter, temperature controlled to 20 °C. CD spectra were evaluated and deconvoluted using convex constraint analysis (CCA) by employing a data set of five pure components as described by Buttani et al. (*30*). Other CD deconvolution tools using the DichroWeb server (http://dichroweb.cryst.bbk.ac.uk/) (*31*) were tested as well as were other data sets of pure components. However, in all cases, the predicted curves deviated much more from the experimental ones as for the deconvolution using the CCA algorithm.

Chromatographic Techniques. Separation and quantification of FAD (flavin adenine dinucleotide), FMN (flavin mononucleotide), and riboflavin was achieved as described previously (*32*).

The determination of the native molecular weights of proteins was achieved by using a BioSep-SEC-S3000 HPLC column in the dimension 300/7.8 (Phenomenex, Aschaffenburg, Germany). A sodium phosphate buffer (200 mM, pH 7.5) containing 150 mM sodium chloride was used as eluent under isocratic conditions (1 mL/min). The elution of the proteins was followed by UV detection at 220 and 280 nm. Calibration and estimation of protein molecular weights were achieved by employing a standard mixture of proteins of known molecular weight (Aqueous Sec 1; Phenomenex, Aschaffenburg, Germany). Prior to injection, equal amounts of the respective LOV protein were dialyzed against 200 mM sodium phosphate buffer, pH 7.5, supplemented with 150 mM sodium chloride. Each sample was injected twice, and at least two independent protein preparations were used for the analysis. The identity of the respective elution peak was verified by its typical LOV (flavin) spectrum.

Homology Modeling and Bioinformatic Analysis. Homology models for the LOV-core domains of PpSB1-LOV and PpSB2-LOV were generated based on the *Chlamydomonas reinhardtii* LOV1 dark state crystal structure (1N9L) (best template according to SwissModel (*24*)). All models were energy minimized by using either the GROMOS96 (*33*) force field implemented in SwissPDB-Viewer (*34*) or the MAB all-atom force field implemented in the MOLOC modeling package (*35*). Evaluation of amino acid side-chain rotamers was performed using WinCoot version 0.1.2 (*36*). The quality of the models was evaluated using the SAVS (structure analysis and validation) server (http://nihserver.mbi.ucla.edu/SAVES/) as described previously (*6*). Sequence alignments were generated using the AlignX tool, implemented in the VectorNTI sequence analysis package. Alignments were visualized and edited manually using the GeneDoc tool (*37*). Phylogenetic analyses were performed using either PhyML (*38*), MultiPhyl (*39*), or IQPNNI (*40*). Bootstrapped maximum-likelihood trees with 100 replicates for each run were generated using the PhyML server and the MultiPhyl server, respectively. Next-neighbor interchange and subtree pruning and recrafting tree searches using 100 bootstrap replicates were performed using MultiPhyl server. Additionally, bayesian posterior probability support values were added to each branch of the ML tree using BEAST v1.4.5 (*41*).

RESULTS

Protein Expression and Biochemical Characterization of the Wild-Type (WT) PpSB1- and PpSB2-LOV Proteins. In contrast to the previously characterized PpSB2-LOV construct (*6*), the PpSB2-LOV construct used in this study lacked the

first three amino acids at the N-terminus of the protein rendering the amino acid numbering for both proteins identical. This short truncation did not alter the spectral properties of the protein nor did it affect the dark recovery rate constant in comparison to the previously reported value.

Both proteins could be expressed in soluble form as N-terminal hexahistidine-tagged fusion proteins. The IMAC purified proteins had a yellow color indicative for the presence of a flavin cofactor. Analytical HPLC-based size-exclusion chromatography revealed an apparent molecular mass of 37.1 kDa for PpSB1-LOV and 39.7 kDa for PpSB2-LOV, which suggests a dimeric organization for both proteins. The calculated molecular masses of the respective monomers are 18.6 kDa for PpSB1-LOV and 19.2 kDa for PpSB2-LOV, both in good agreement with the monomer band observed in denaturing SDS−PAGE analysis (not shown). The chromophore content of purified PpSB1-LOV and PpSB2-LOV was determined by protein denaturation, extraction, and HPLC analysis. The HPLC analysis revealed that PpSB1-LOV binds predominately FMN (96 ± 4%) with minor traces of FAD (4 ± 0%). Contrarily, PpSB2-LOV contains a mixture of FMN (70 ± 3%), riboflavin (26 ± 8%), and traces of FAD (4 ± 0%).

Spectroscopic Studies and Recovery Kinetics of Wild-Type PpSB1/2-LOV Proteins. In the dark, both proteins exhibit the typical LOV-like UV/vis spectra (Figure 1) with very similar absorption maxima in the blue region around 450 nm indicative of a noncovalently bound flavin species (LOV447). In the UVA region, the spectrum of PpSB1-LOV shows a maximum at 376 nm (Figure 1A, upper panel) much like isolated YtvA-LOV (*42*), whereas the band for PpSB2-LOV is slightly blue shifted and broader with a double peak structure at 350 and 370 nm (Figure 1B, upper panel). Upon blue light illumination the absorption band in the visible region decreases for both proteins, although for PpSB2-LOV the photoproduct (LOV390) cannot be accumulated to 100%. The recovery of the dark state (LOV447) for both proteins was recorded at 480 nm after blue light illumination (Figure 1). The experimental data can best be fitted using a double exponential decay function, yielding two time constants, $\tau_1 = 113 \pm 7$ min ($A_1 = 2.2 \pm 0.1\%$) and $\tau_2 = 2525 \pm 22$ min ($A_2 = 97.8 \pm 0.5\%$) for PpSB1-LOV. Double exponential fitting of the kinetic trace for PpSB2-LOV resulted in $\tau_1 = 28 \pm 2$ s ($A_1 = 29.5 \pm 2\%$) and $\tau_2 = 184 \pm 15$ s ($A_2 = 70.5 \pm 1\%$). According to the formula $\tau_{rec} = \sum A_i \tau_i / 100$, this results in average dark recovery time constants of $\tau_{rec} = 2471 \pm 22$ min for PpSB1-LOV and $\tau_{rec} = 137 \pm 11$ s for PpSB2-LOV (at 20 °C). The latter value is well in accordance with the previously reported value for PpSB2-LOV of $\tau_{rec} = 114$ s (*6*). All measurements were at least performed twice for two independent protein preparations of PpSB1-LOV and three times each for two independent preparations of PpSB2-LOV. The experimental error associated with τ_{rec} was about 10%.

Sequence Analysis and Mutational Strategy To Modifiy Dark Recovery Kinetics. The two proteins are highly similar in sequence (about 66% identity). Both possess short N- and C-terminal extensions of the LOV-core domain. To address the mechanistic reason for the drastically different dark recovery kinetics, a mutational analysis was carried out. A multiple sequence alignment of PpSB1-LOV and PpSB2-LOV highlighting the introduced mutations together with the sequences of YtvA-LOV and AsLOV2 is shown in Figure 2.

The selection of amino acid positions that were mutated in this study was based on a sequence alignment that included both PpSB1-LOV and PpSB2-LOV sequences and a selection of fast reverting phototropin LOV2 domains as well as sequences of the slow reverting FKF1/LKP2/ZTL LOV family (*21*) (Supporting Information Figure 1). Based on this alignment, amino acid positions were chosen that differ between PpSB1-LOV and PpSB2-LOV and, moreover, are different in the fast reverting phototropin LOV domains and the slow reverting FKF1/LKP2/ZTL LOV proteins. From a homology model generated for PpSB2-LOV (*6*), which is based on the *C. reinhardtii* LOV1 structure (PDB entry 1N9L), amino acid positions in a distance of 6 Å from the FMN chromophore were chosen for mutual interchange between PpSB1-LOV and PpSB2-LOV (highlighted in Figure 2). Hence, when the mutation A13H was generated in PpSB1-LOV, the corresponding H13A mutation was generated in PpSB2-LOV. Six mutations were generated for each of the two proteins: A13H, K23Q, E47D, R61H, R66I, and K71E for PpSB1-LOV and the respective exchanges in PpSB2-LOV. The most pronounced sequence differences between PpSB1-LOV and PpSB2-LOV are found in the extensions C-terminal to the LOV-core domain (Figure 2). Accordingly, the C-terminal portions were interchanged between both proteins. The respective variant termed cSB1/αSB2 contains the PpSB1-LOV core domain (residues 1−118) and the extension of PpSB2-LOV, and *vice versa* the variant cSB2/αSB1 consists of the LOV-core domain of PpSB2-LOV (residues 1−118) and the C-terminal extension of PpSB1-LOV. In summary, this strategy resulted in 12 different constructs, each carrying a single specific amino acid exchange and two mutants with interchanged C-terminal extensions.

Small-Scale Prescreening of PpSB1-LOV and PpSB2-LOV Mutants. Small-scale expression cultures were grown as described in Materials and Methods. The crude cell extracts of mutants together with the respective wild-type proteins were initially analyzed for changes in their dark recovery kinetics using a microtiter plate based assay. The recovery for the wild-type PpSB2-LOV protein was determined under these conditions as 106 ± 4 s, in good agreement with the time constant previously observed for the purified protein (*6*). For three mutants, a strong deviation from the WT behavior was found: PpSB2-H61R (731 ± 20 s), -I66R (1760 ± 16 s), and cSB2/αSB1 (338 ± 8 s). All other PpSB2-LOV mutants showed negligible to minor changes with respect to the WT protein (-H13A, -Q23K, -D47E, -E71K). Due to the slow recovery of PpSB1-LOV ($\tau_{rec} = 2471$ min at 20 °C), it was difficult to record dark recovery time traces for the respective mutant proteins as well as for the wild-type using our prescreening approach in microtiter plates. The dark recovery for the PpSB1-LOV mutants was therefore monitored for 3 h only. In this way it was possible to identify three faster reverting mutants, which showed exponential kinetics within 3 h of measuring time (Table 1). Interestingly, the variants identified carried the mutations at the same amino acid positions which were previously identified for PpSB2-LOV to slow down the recovery. Mutants identified were PpSB1-R61H (109 ± 4 min), -R66I (5.9 ± 0.1 min), and cSB1/αSB2 (263 ± 12 min). Therefore, these three PpSB1-LOV mutants and the three corresponding PpSB2-LOV mutants were chosen for purification and further characterization.

Purification and Characterization of PpSB1-LOV and PpSB2-LOV Mutant Proteins. All mutant proteins were expressed and purified as described for the respective wild-type proteins. All proteins exhibited typical LOV-like UV/vis spectra (see Supporting Information Figure 2). Spectral changes between mutated and wild-type proteins were minor, and the protein-to-chromophore ratio was in most cases close to 1. The

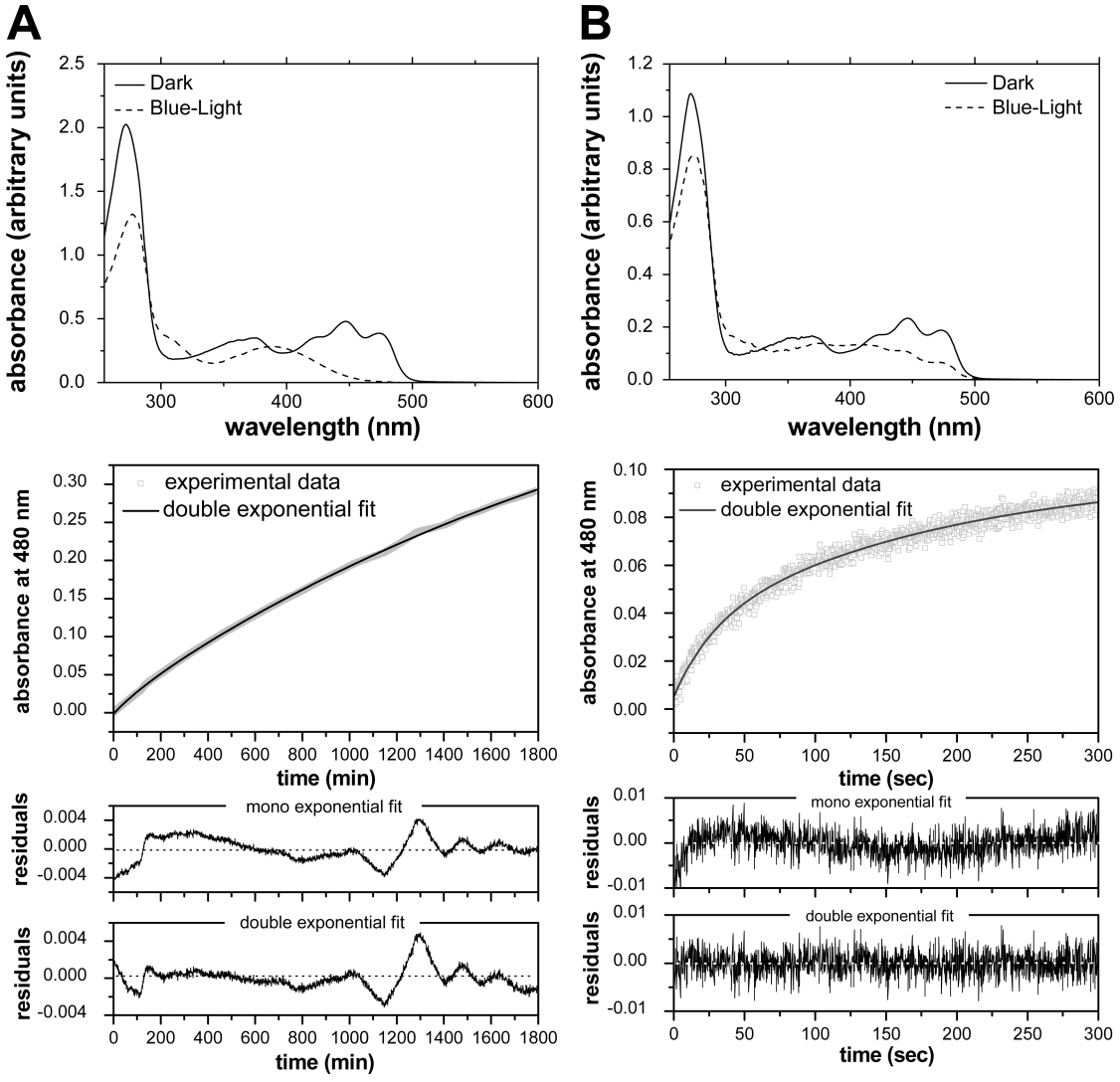

FIGURE 1: Blue light sensitivity and photochemistry of wild-type PpSB1-LOV (A) and PpSB2-LOV (B). The UV/vis absorbance spectra for the dark state of both proteins are shown as a solid line, and the corresponding absorbance spectra after illumination with blue light are depicted as a dashed line (upper panel). Below the UV/vis spectra the dark recovery time traces recorded at 480 nm absorbance for the respective protein after blue light illumination for 30 s are shown. The experimental data are depicted with open squares (in gray); solid lines (in black) indicate the double exponential fit of the data. The two lower panels give the residual distribution for a single and double exponential fit of the experimental data, respectively. Residuals are better distributed for the double exponential fit, especially in the shorter time region; thus, the dark recovery time traces were fitted using a double exponential decay curve.

chromophore content was assessed from the UV/vis spectra (absorption ratio 272 nm/447 nm) as described previously (*43*). The kinetics of the dark state recovery for all mutant proteins were determined in triplicate for at least two independent preparations (Table 2).

For both proteins, the mutation at position 66 has the strongest influence on dark recovery (PpSB1-R66I, PpSB2-I66R), accelerating the lifetime from 2471 ± 22 min (41.2 h) for PpSB1-LOV to about 23 ± 1 min in the case of PpSB1-R66I. This represents an acceleration of the dark recovery by roughly 2 orders of magnitude. Conversely, the corresponding I66R mutation in PpSB2-LOV shows the strongest effect of all analyzed PpSB2-LOV mutants. The dark recovery in the latter case is slowed down by a factor of about 7 from 137 ± 11 s (PpSB2-LOV) to 975 ± 363 s (PpSB2-I66R).

The mutation R61H in PpSB1-LOV accelerates the dark recovery by a factor of about 3 (from 2471 ± 22 min to 765 ± 589 min), whereas the corresponding H61R mutation in PpSB2-LOV slows the recovery down to 581 ± 237 s (by a factor of about 4).

The mutual exchange of the C-terminal extensions of PpSB1-LOV and PpSB2-LOV, resulting in cSB1/αSB2 and cSB2/αSB1, also had a pronounced effect on the dark recovery of the two proteins. The recovery time constant of cSB1/αSB2 was about 2 times faster (1330 ± 448 min) compared to PpSB1-LOV (2471 ± 22 min). Conversely, the recovery of cSB2/αSB1 was slowed down by a factor of 3 from 137 ± 11 s for the WT protein to 444 ± 39 s for cSB2/αSB1. It should be noted here that the dark recovery time constants determined for the purified proteins (Table 2) differed quantitatively (but not qualitatively) from the values obtained with measurements using crude cell extracts (Table 1). For example, the mutant PpSB1-R66I displayed a 369-fold acceleration in crude cell extracts. In contrast, the purified mutant protein only showed a 107-fold acceleration of the dark recovery. The same holds true for all analyzed variants with the kinetic effects being more pronounced in crude extracts.

Chromophore Acceptance and Oligomerization of PpSB1-LOV and PpSB2-LOV Proteins. The flavin chromophore content and composition were analyzed for all mutant

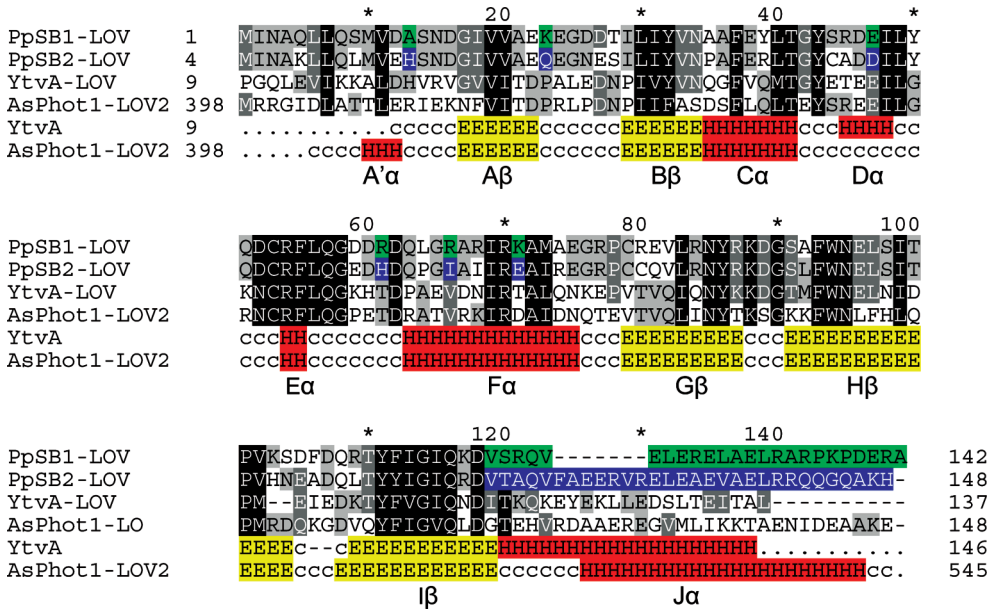

FIGURE 2: Sequence alignment of PpSB1-LOV, PpSB2-LOV, *B. subtilis* YtvA-LOV, and *A. sativa* phot1-LOV2. The PpSB2-LOV construct used throughout this study lacked the first three amino acids compared to the previously described construct and the sequence in the database (Q88JB0). Introduced point mutations are highlighted in green for PpSB1-LOV and blue for PpSB2-LOV. The mutually exchanged C-terminal extensions are highlighted in both sequences. Identical amino acids are shaded in black; similar amino acids are shaded in dark (above 80% conservation) and light gray (under 60% conservation). Below the alignment the assignment of secondary structure elements is shown for AsLOV2 and YtvA using the numbering according to the YtvA-LOV crystal structure. α-Helices (H) are marked in red, *β*-strand structures (E) are highlighted in yellow, and random coil elements (c) are depicted in white.

Table 1: Dark Recovery Time Constants Observed in the Small-Scale Prescreening Using Crude Cell Extracts of All PpSB2-LOV and PpSB1-LOV Proteins

protein	τ_{rec} (min)[b]	protein	τ_{rec} (s)[a]	*x*-fold change
PpSB1-LOV	nd	PpSB2-LOV	106 ± 4	
PpSB1-A13H	nd	PpSB2-H13A	189 ± 4	+1.8
PpSB1-K23Q	nd	PpSB2-Q23K	355 ± 7	+3.3
PpSB1-E47D	nd	PpSB2-D47E	153 ± 5	+1.5
PpSB1-R61H	109 ± 4	PpSB2-H61R	731 ± 20	+7
PpSB1-R66I	6 ± 0	PpSB2-I66R	1760 ± 16	+16
PpSB1-K71E	nd	PpSB2-E71K	293 ± 4	+2.7
cSB1/αSB2	263 ± 12	cSB2/αSB1	388 ± 8	3.6

[a]Values derive from triplicate measurements for the same crude cell extract. [b]For PpSB1-LOV wild type and certain slow reverting variants the dark recovery kinetics could not be determined (nd) in crude cell extracts because the recovery time traces did not obey a monoexponential decay over a measuring time of 3 h. In particular, for the wild-type PpSB1-LOV protein it was impossible to assess the dark recovery time constant using small-scale prescreening. Therefore, no values for the change in the respective time constant (*x*-fold change) could be derived for the PpSB1-LOV mutant proteins. For comparison, the purified wild-type PpSB1-LOV proteins show a dark recovery time constant of 2212 min at 20 °C.

and wild-type proteins (Table 2). All PpSB1-LOV proteins bound predominately FMN as chromophore. Whereas most mutant proteins did not exhibit any change in their chromophore preference, the PpSB2-I66R mutant exhibited a PpSB1-LOV-like chromophore content, binding only FMN. In contrast, PpSB2-LOV accepts both FMN and riboflavin in a ratio of 70/30. Conversely, the corresponding PpSB1-R66I mutant did not exhibit any change in chromophore composition, binding only FMN, like all other PpSB1-LOV preparations.

Size-exclusion chromatography was performed to elucidate the native oligomerization state of the respective mutant proteins. In all cases, the analysis revealed a dimeric organization with a retention time (within the uncertainty of the method) identical to the values observed for the respective wild-type proteins.

Tryptophan Fluorescence Measurements To Probe Local Structural Changes Due to Introduction of the Mutations. Both proteins possess a single tryptophan (W94) residue localized on the LOV core and conserved among most LOV proteins. Therefore, W94 in both proteins represents a sensitive probe for local structural changes that might be introduced by the mutation. Tryptophan fluorescence spectra were recorded after excitation at 295 nm and were normalized for the amount of absorbed energy at the excitation wavelength (Figure 3). The Trp emission maximum of PpSB2-LOV (338 nm) is red shifted by about 3 nm compared to PpSB1-LOV (341 nm). Interestingly, the interchange of the C-terminal extensions between the two proteins results in a correlated shift of the Trp fluorescence maxima. In cSB2/αSB1 the emission maximum is red shifted by about 4 to 342 nm. *Vice versa*, cSB1/αSB2 has a Trp emission maximum (337 nm) which is blue shifted by about 3 nm compared to PpSB1-LOV (341 nm).

Whereas the R66I mutation in PpSB1-LOV had practically no effect on the Trp emission maximum (340 nm compared to 341 nm in the wild-type protein), the corresponding I66R mutation in PpSB2-LOV resulted in a red shift of the emission maximum to 341.5 nm in comparison to the wild type (338 nm). The H61R (PpSB2-LOV) and the respective R61H (PpSB1-LOV) mutation had no effect on the emission maximum of W94.

CD Spectroscopy of WT and Mutant Proteins. For all proteins used in this study, CD spectra were recorded in the dark and after 30 s of blue light illumination. CD spectra of the two wild-type LOV proteins and the mutants possessing interchanged C-terminal extensions are shown in Figure 4.

Spectra were smoothened and used for deconvolution applying the CCA (convex constraint analysis) algorithm implemented in the CCA$^+$ tool (*25*). For deconvolution we used the data set

Table 2: Dark Recovery Time Constants and Observed Chromophore Acceptance for Mutant and Wild-Type LOV Proteins

	dark recovery kinetics		chromophore acceptance		
protein	τ_{rec} [a]	*x*-fold change	FMN (%)[b]	riboflavin (%)[b]	FAD (%)[b]
PpSB1-LOV	2471 ± 22 min		96.0 ± 4.0	nd	3.5 ± 0
PpSB1-R66I	23 ± 1 min	−107	100 ± 0	nd	nd
PpSB1-R61H	765 ± 589 min	−3	99.1 ± 1.2	0.9 ± 0	nd
cSB1/αSB2	1330 ± 448 min	−2	100 ± 0	nd	nd
PpSB2-LOV	137 ± 11 s		70.3 ± 3.0	26.0 ± 8.0	3.7 ± 0
PpSB2-I66R	975 ± 363 s	+7	100 ± 0	nd	nd
PpSB2-H61R	581 ± 237 s	+4	22.2 ± 3.0	53.9 ± 5.3	23.6 ± 2.1
cSB2/αSB1	444 ± 39 s	+3	65.4 ± 1.9	26.7 ± 1.0	7.9 ± 2.7

[a]Values derive from triplicate measurements on at least two independent preparations. In most cases a double exponential decay curve best fitted the kinetic data. The reported average τ_{rec} values were derived from the sum of the two exponential time constants τ_1 and τ_2 according to the formula $\tau_{rec} = \sum A_i\tau_i/100$. For certain preparations the standard deviation resulting from the measurement of two independent preparations is exceeding 10%. This is apparently due to a variation between the different preparations for the same mutant protein. However, the overall trend regarding the acceleration or deceleration remains the same even within the large associated error. [b]Values derive from triplicate measurements on at least two independent preparations. nd: not detectable. A standard deviation of 0% results when one of the flavin species (e.g., FAD) could only be detected in one of the two independent preparations.

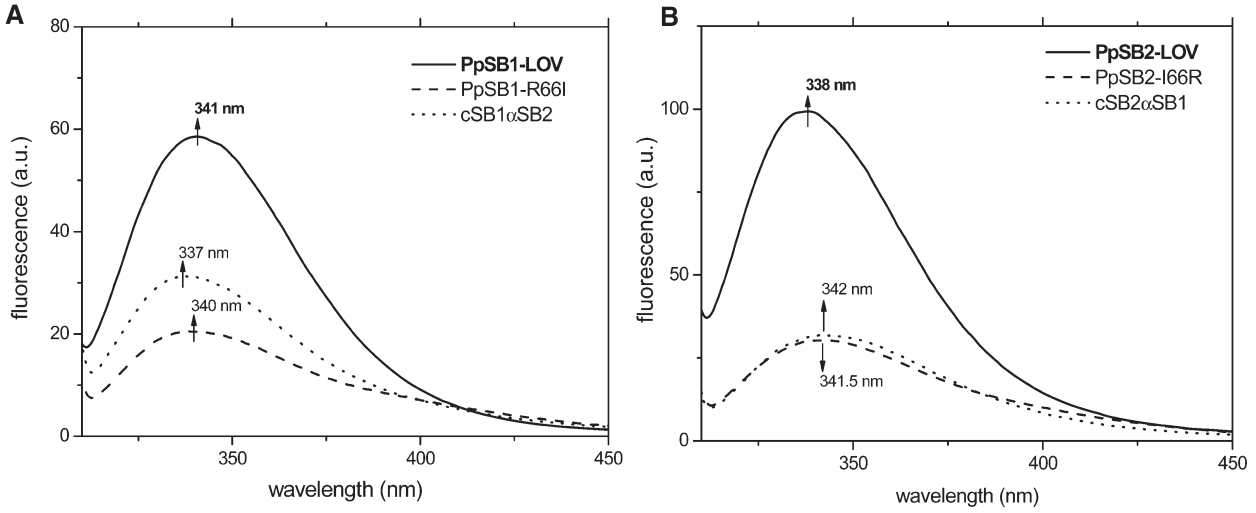

FIGURE 3: Fluorescence emission spectra of W94 for PpSB1-LOV (A) and PpSB2-LOV (B) and in the respective mutant proteins after excitation at 295 nm. The Trp emission spectra for the wild-type proteins are shown with solid lines. PpSB1-R66I and PpSB2-I66R are drawn in dashed lines. The spectra for the mutants with interchanged C-terminal extensions (cSB1αSB2 and cSB2αSB1) are depicted with dotted lines. In all cases the emission maxima are marked by an arrow.

employed by Buttani et al. (*30*) that assumes five pure components: (i) α-helices, (ii) turns and other structures, (iii) parallel/twisted *β*-sheets, (iv) random coils, and (v) antiparallel *β*-sheets. For all proteins the obtained CD spectra could be fitted well with the theoretically CCA-predicted curves. The total average rmsd between the calculated and experimental spectrum was in all cases well below 5%. All variants (even the mutants with the interchanged C-terminal extensions) (Figure 4) exhibit very similar CD spectra to the respective wild-type proteins (see Supporting Information Figure 3). For the two wild-type proteins, Table 3 summarizes the CCA analysis derived percentages for the five pure components. Table 4 shows a comparison between the theoretically expected secondary structure composition and the CD-derived values for the two wild-type LOV proteins. For both wild-type proteins and all mutants the differences between dark and light state CD spectra were small.

We compared the CD-derived secondary structural predictions for the two full-length *Pseudomonas* LOV proteins to known LOV domains by analyzing a set of currently available LOV domain crystal structures with respect to their content of α-helices, *β*-strands, and coil/turn structures (Table 4). On average, LOV-core domains (consisting of about 105 aa) contain about 27 amino acids in helical conformation, consist of about 40 aa *β*-strands, and contain 38 aa coils/turns and other structures.

As evident from Table 4, the CD-derived content of α-helices with about 45−47 aa for the two proteins clearly exceeds the theoretically expected value of 27 amino acids. The number of amino acids that in both *Pseudomonas* proteins constitute the *β*-scaffold closely matches the expected values. In both proteins, the number of amino acids in coil/turn structures exceeds the expected value by about 20, which is readily accounted for by the 20 amino acid long N-terminal tag and the introduced thrombin site (sequence: MGSSHHHHHH-SSGLVPRGSH).

DISCUSSION

Site-Directed Mutagenesis Combined with Microtiter Plate Prescreening Readily Identified Amino Acids Influencing the Dark Recovery. Our mutagenesis and prescreening strategy readily identified a number of PpSB1-LOV and PpSB2-LOV variants with altered dark recovery kinetics. Prescreening in microtiter plates allows for a fast and easy evaluation of the dark

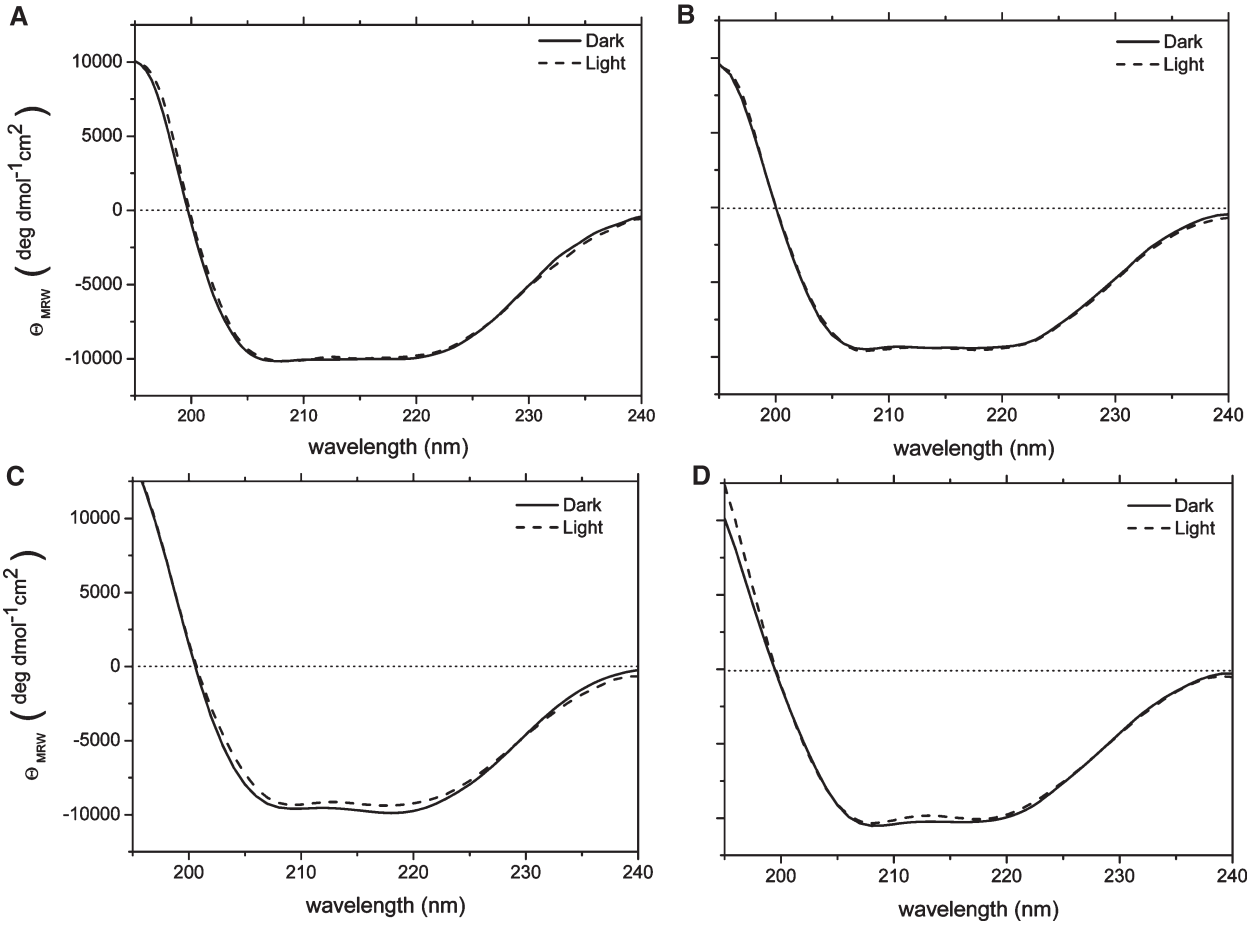

FIGURE 4: Far-UV CD spectra recorded for wild-type PpSB1-LOV (A) and PpSB2-LOV (B) as well as for cSB1/αSB2 (C) and cSB2/αSB1 (D). The depicted spectra represent the mean of two independent measurements on two different preparations. Spectra for the dark-adapted proteins are shown in solid lines whereas the corresponding spectra after 30 s of blue light illumination are depicted with dashed lines.

Table 3: Results of the CCA Analysis on CD Spectra

protein	α-helix (%)	turn and others (%)	twisted or parallel β-sheets (%)	random coil (%)	antiparallel β-sheets (%)
PpSB1 dark	29.0 ± 1.8	22.7 ± 1.6	13.5 ± 0	21.4 ± 2.6	13.5 ± 2.8
PpSB1 light	29.6 ± 1.0	22.5 ± 1.6	14.5 ± 0.3	20.9 ± 1.9	12.6 ± 1.0
PpSB2 dark	26.5 ± 0.7	23.0 ± 3.3	15.7 ± 0.5	19.3 ± 2.1	15.6 ± 1.1
PpSB2 light	26.5 ± 0.7	22.5 ± 2.6	16.2 ± 0.4	19.3 ± 1.3	15.6 ± 1.1

recovery kinetics of mutated LOV proteins without the need for protein purification. This strategy should be amenable to even higher throughput by cultivating mutant LOV protein expressing clones, e.g., derived from a mutant library (*26*), in 96-well deep-well plates. However, care has to be taken when interpreting the dark recovery time constants derived using such crude cell extracts. We observed quantitative but not qualitative differences between the values obtained with crude cell extracts and those with purified proteins. A similar effect has previously been observed for mutants of *B. subtilis* YtvA protein (A. Losi, personal communication). Thus, it appears that certain components in the *E. coli* crude extracts influence the dark recovery of LOV proteins. Nevertheless, such a prescreening approach, in particular when combined with microtiter plate cultivation, enables a fast and efficient selection of LOV mutants with altered photochemical reactivities. UV/vis spectroscopy (Supporting Information Figure 2) and CD spectroscopy (Figure 4 and Supporting Information Figure 3) performed on the respective purified wild-type and mutant proteins revealed proper folding of all constructs used throughout this study.

Protein−Chromophore Interactions around the FMN Phosphate Stabilize the Adduct State of LOV Domains. The amino acid in position 66 strongly influences the dark recovery in both proteins in a correlated manner. Moreover, in PpSB2-LOV, this mutation also affects the chromophore preference toward a PpSB1-LOV-like behavior (accepting only FMN) whereas the wild-type protein accepts both FMN and riboflavin in a ratio of 70/30. This in fact implies a physical interaction between R66 in PpSB1-LOV and the FMN phosphate. Whereas the mutation R66I in PpSB1-LOV accelerates the dark recovery of the mutant by 2 orders of magnitude, the corresponding mutation in PpSB2-LOV (I66R) slows down the recovery by roughly 1 order of magnitude. Interestingly, the corresponding mutation in PpSB1-LOV (R66I) does not result in a change of chromophore acceptance. This suggests additional structural components adding to the very slow dark

Table 4: Comparison between Expected and CD Predicted Secondary Structure Composition

protein	no. of amino acids		
	α-helix	β-strands	coils/turns/ others
consensus LOV core[a] (105 residues)	27 ± 1.8	40 ± 2.6	38 ± 4
PpSB1-LOV[b] (162 residues)	47 ± 3	44 ± 4	71 ± 3
PpSB2-LOV[b] (168 residues)	45 ± 1	54 ± 1	71 ± 5

[a]The expected secondary structure content for LOV domains was inferred from the available dark state structures. All crystal structures were truncated for the consensus LOV-core domain. Secondary structure content was predicted by using the DSSP algorithm. PDB coordinates: 1G28, 1N9O, 2PR5, 2V1A, 2Z6C, and 2Z6D. [b]For the full-length proteins PpSB1-LOV and PpSB2-LOV the number of amino acids in a given conformation are derived from two sets of CD measurements on two different preparations.

recovery time constant of PpSB1-LOV as well as to the strong preference for FMN.

The inspection of the homology models generated for the two LOV-core domains (for details see Materials and Methods) revealed that R66 in PpSB1-LOV is readily brought within hydrogen-bonding distance to the FMN phosphate by simply adjusting favorable rotamers (Figure 5A). The corresponding side chain, I66 in PpSB2-LOV, is apparently not able to contact the FMN phosphate in a similar manner (Figure 5B).

Laser-induced optoacoustic spectroscopy (LIOAS) on LOV domains and proteins revealed a high energy content of the photoadduct LOV390, e.g., 180 kJ/mol for *C. reinhardtii* LOV1 (CrLOV1) and 136 kJ/mol for *B. subtilis* YtvA indicating that the photoproduct stores more than 55% of the 0-0 energy (246.5 kJ/mol) (*44*). This high energy content of LOV390 ensures the enthalpic driving force for completion of the photocycle. In the dark state of LOV domains and in CrLOV1, the FMN phosphate is stabilized by hydrogen bonds and/or salt bridges with amino acids R58 and R74 corresponding to R54 and R70 in PpSB1-LOV and PpSB2-LOV, respectively (see Figure 5). Upon formation of the adduct state, the lateral chain of R58 in CrLOV1 moves slightly away from the FMN ribityl chain, resulting in a distance change between the FMN phosphate and R58. Concomitantly, the weak interactions between R74 and the FMN phosphate are strengthened. These movements help in stabilizing the adduct state and must be reversed for completion of the photocycle in the dark. Furthermore, Losi and co-workers demonstrated that the mutation of one of the two arginines that coordinate the FMN phosphate (R58, in CrLOV1) to lysine accelerated the dark recovery about 3-fold (*44*). A similar effect was observed for the corresponding mutation R63K in YtvA, where the recovery is accelerated 8-fold from 3900 to about 480 s at 20 °C (A. Losi, personal communication; Y. Tang, Z. Cao, E. Livoti, U. Krauss, K.-E. Jaeger, W. Gärtner, and A. Losi, submitted for publication). For CrLOV1 and YtvA, it was thus concluded that the substitution R58K hinders the conformational rearrangements around the FMN phosphate, as confirmed also by LIOAS data, destabilizing the adduct state and inducing the faster recovery of the respective mutant proteins. In PpSB1-LOV, residue R66 is located close to the second arginine coordinating the FMN phosphate (R74 on helix Fα in CrLOV1, R70 in PpSB1-LOV) and is thus located opposite to the photoactive cysteine and R54 (on helix Eα, corresponding to R58 in CrLOV1 and R63 in YtvA). In light of our data, one can speculate that in the adduct state of PpSB1-LOV, not only the

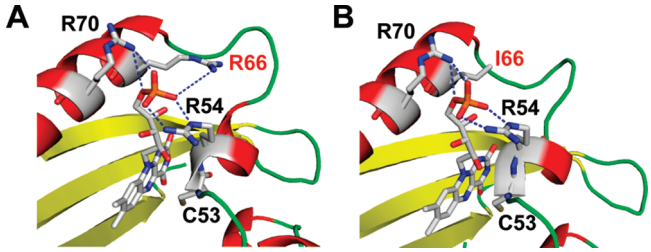

FIGURE 5: View of the FMN-binding pocket and the protein region surrounding the FMN phosphate for PpSB1-LOV and PpSB2-LOV, respectively. Both figures are derived from homology models of the PpSB1-LOV (A) and the PpSB2-LOV (B) LOV-core structures. The *C. reinhardtii* LOV1 structure (1n9O) was selected as template. The two highly conserved arginine residues (R54 and R70 in both proteins) that coordinate the FMN phosphate are labeled and shown in stick representation. The photoactive cysteine residue (C53 in both proteins) involved in the light-dependent adduct formation between the protein and the flavin-isoalloxazine ring is included for orientation. Additionally, the amino acid in position 66 in both *Pseudomonas* LOV proteins (R66 in PpSB1-LOV and I66 in PpSB2-LOV) is highlighted.

interaction with R70 (R74 in CrLOV1) is strengthened but also the interaction with R66. These rearrangements might further stabilize the adduct, e.g., by relieving some of the strain imposed on the protein/chromophore assembly present in the adduct state that results from the covalent linkage of the flavin isoalloxazine ring to the photoactive cysteine. This in turn results in a very slow dark recovery of the PpSB1-LOV protein. *Vice versa*, the absence of the stabilizing interaction in PpSB2-LOV and PpSB1-R66I results in a faster dark recovery much like in phot LOV domains. Studies on PpSB1-LOV and PpSB2-LOV using optoacoustics and the determination of the energy content of LOV390 in the two proteins would help to understand the peculiar features of the photocycle of two *P. putida* proteins and advance our understanding of the photochemistry of bacterial LOV proteins.

Notably, in the vast majority of LOV domains this position on helix Fα is occupied by a hydrophobic amino acid, which does not influence the recovery kinetics (e.g., V75 in YtvA, V462 in As-phot1 LOV2). The only other very slow reverting LOV domains of the FKF1/LKP2/ZTL LOV family (τ_{rec} = 62.5 h at room temperature) (*21*) contain a valine at the position corresponding to R66 in PpSB1-LOV; thus the very slow recovery of the FKF1 LOV proteins must result from a different mechanism as suggested here for the *P. putida* LOV proteins. Zikihara and co-workers speculated that the slow reversion may derive from the nine amino acid insertion to the LOV-core amino acid sequence between helix Eα and Fα. Notably, the latter two helices harbor the two arginines discussed above that in all LOV domains coordinate the FMN phsophate. Thus, it is tempting to speculate that the orientation of amino acids around the FMN phosphate, e.g., influenced by the insertion found in FKF1 LOV between Eα and Fα, might result in a stabilization of the adduct state and hence result in a very slow dark recovery reaction. In conclusion, the dependency of the dark recovery on the amino acid in position 66 in PpSB1-LOV and PpSB2-LOV must be a peculiar feature of the two *Pseudomonas* LOV proteins. However, the general mechanism of tuning the dark recovery by an intricate network of amino acids surrounding the FMN phosphate might well be a conserved mechanism present in all LOV domain systems.

In PpSB1-LOV and PpSB2-LOV the Dark Recovery Is Not Driven by Steric Constraint. Recently, Christie and co-workers could show that steric constraint can tune the dark

recovery kinetics in LOV domains, although mechanistically acting from the opposite side of the FMN-binding pocket (*26*). They identified one amino acid residue (I427, As-phot1 numbering) located in van der Waals contact with the sulfur atom of the photoreactive cysteine (C450). An exchange of this residue by valine accelerates the dark recovery 10-fold and slows down the adduct formation by a factor of 2 as revealed by laser flash photolysis measurements. The authors thus concluded that steric interactions in the protein around the FMN chromophore, specifically close to the photoreactive cysteine residue, can influence the dark recovery process either by stabilizing the adduct or by facilitating its decay. To address the latter issue for PpSB1-LOV and PpSB2-LOV, we have performed an investigation of the adduct formation kinetics of the two wild-type LOV proteins by time-resolved laser flash photolysis (Supporting Information Figure 6). The measurement did not reveal any major difference in the adduct formation kinetics for the two wild-type proteins. In PpSB1-LOV and PpSB2-LOV the FMN triplet (LOV660) decays to the adduct state with a time constant of 1.5 and 1.6 μs, respectively. Thus, we can rule out the involvement of a similar recovery-driving mechanism based on steric constraint in the FMN-binding pocket of the two *P. putida* LOV proteins. More likely, the adduct seems to be stabilized by the strengthened interaction of R66 and the FMN phosphate in PpSB1-LOV and PpSB2-I66R and destabilized in PpSB2-LOV and PpSB1-R66I. This stabilization versus destabilization then results in slow versus fast dark recovery reactions.

The Role of Histidines in the Dark Recovery. The effect of the mutation at position 61 (located about 6 Å from the FMN N5 in a loop connecting Eα and Fα helices) in both proteins would argue for a mechanism as proposed by Alexandre and co-workers (*25*). The authors suggested histidine-driven base catalysis from a surface-exposed His residue in quite some distance to the FMN chromophore via a hydrogen-bonding network. The kinetic effect (3−4-fold change) observed for the R61H mutation in PpSB1-LOV and the H61R mutation in PpSB2-LOV, respectively, showed about the same order of magnitude as reported by Alexandre et al. (2-fold change). Here, the authors blocked the histidines of AsLOV2 with diethyl pyrocarbonate (DEPC), a histidine-specific modifying agent resulting in a slowed dark recovery. However, this putative mechanism seems to be much less effective in the two *Pseudomonas* LOV proteins, compared to the tuning of the dark recovery by the FMN phosphate/protein interaction. Thus, at least H61 in PpSB2-LOV is not solely responsible for the fast dark recovery of the protein. It should be noted here that PpSB2-LOV possesses four histidines (one in the N-terminal extension (H13), two in the LOV core (H61, H103), and one in the C-terminal extension (H148)) whereas PpSB1-LOV contains none. The mutation of the second His residue in PpSB2-LOV (H13) had no apparent effect on the recovery of PpSB2-LOV whereas the corresponding mutation A13H in PpSB1-LOV renders the recovery even slower compared to the wild-type protein (data not shown). The two other histidines H103 and H148 were not considered for mutation due to their large distance to the FMN molecule.

The Partially Helical LOV-Core Extensions Influence the Recovery of Both Pseudomonas LOV Proteins but Do Not Undergo Pronounced Conformational Changes. In the far-UV region both wild-type proteins possess typical CD spectra of proteins rich in α-helical and β-sheet content (*45*) much like other LOV proteins for which CD data are available (*30*, *46*−*48*). We are aware that CD spectroscopy is not a precise method for the determination of secondary structure content. In particular, the spectra of pure α-helices and antiparallel β-sheet structures are very similar and thus sometimes difficult to separate during deconvolution. Nevertheless, based on previous data and component curve assignments (*30*), our CD spectra suggest that in PpSB1-LOV and PpSB2-LOV about 20 amino acids in the N- and C-terminal extensions should be in a helical conformation. Under the assumption of a canonical LOV fold, the N- and C-terminal extensions account for about 40 residues which may thus adopt a partial helical structure. In comparison, the N- and C-terminal extensions of the monomeric LOV construct of *A. sativa* phot1-LOV2 that was recently crystallized (PDB access code 2v1a) contain in sum about 24 amino acids in a helical conformation. In the dimeric *B. subtilis* YtvA-LOV crystal structure (2pr5), which is so far the only structure available for a bacterial LOV protein, the C-terminal extension to the LOV core contains about 18 amino acids in a helical conformation. Thus, despite the lack of sequence similarity between the corresponding protein regions, similar structural elements, namely, an N-terminal helical cap structure and a C-terminal Jα helix, appear to be present outside of the conserved LOV core in different plant and bacterial LOV proteins. However, the orientation of the C-terminal Jα helix in the two *Pseudomonas* LOV proteins cannot be resolved without additional structural information. For plant phototropins, the LOV2 associated Jα helix was suggested to promote signaling from the LOV2 domain to the phot kinase (*49*). This notion was based on solution NMR studies (*49*−*51*), indicating that light triggers the displacement or unfolding of the C-terminal Jα helix that connects the LOV2 domain to the kinase in full-length phot. This in turn results in the autophosphorylation of the phot kinase and might allow for downstream signaling and initiation the phototrophic response. For plant LOV2 systems, this model has also found support through CD spectroscopy (*47*, *48*) and time-resolved thermal grating and thermal lens experiments (*52*). However, for bacterial LOV systems, so far no light-dependent loss of helical content could be observed using CD spectroscopy (*30*). Similar to those latter observations, we did not observe any significant light-dependent loss of helicity for the two *P. putida* LOV proteins. However, on the basis of CD data alone we cannot rule out that a structural rearrangement takes place which is not accompanied by a loss of secondary structure, e.g., involving a movement or the rotation of the helices.

Influence and Orientation of the C-Terminal Extension. In this study, only the C-terminal (Jα helix) extensions of PpSB1-LOV and PpSB2-LOV were interchanged between the two proteins as the extensions N-terminal to the LOV core did not differ significantly in their amino acid sequence. This exchange had a pronounced effect on the recovery of PpSB1-LOV and PpSB2-LOV, accelerating the recovery of cSB1/αSB2 by a factor of 2 and slowing down the recovery of cSB2/αSB1 by a factor of 3 with respect to the wild-type proteins. The kinetic effect of interchanging the C-terminal extensions on the dark recovery process, as well as the influence of the interchange on the spectral properties of the sole Trp residue (W94), is clear evidence for an interaction of the C-terminal extension with residues that directly or indirectly interact with the FMN chromophore. The latter result moreover indicated that the respective extensions are located close to W94 in both proteins. A "helix-out" orientation, as in the crystal structure of YtvA-LOV (*53*) (Supporting Information Figure 5C), would nicely account for the observed phenomena, since W103 in YtvA-LOV and the corresponding

W94 in both *Pseudomonas* LOV proteins are in close proximity to the Jα extension in a "helix-out" conformation. Still, in the AsLOV2 structure, where the Jα helix packs against the LOV-core β-scaffold in a "helix-in" conformation, the sole Trp (W491, As-phot1 numbering) similarly contacts the Jα helix in a hinge region that connects the AsLOV2 core to the Jα helix (Supporting Information Figure 5D) (*54*). When we align the respective C-terminal extensions of PpSB1-LOV and PpSB2-LOV to the corresponding Jα helix in either YtvA-LOV or AsLOV2 (not shown), a higher similarity to the Jα helix of YtvA-LOV (about 20% identical and 40% similar positions) compared to AsLOV2 (15% identical and 21% similar positions) is detected. This, together with the dimeric organization of the two proteins (YtvA LOV is dimeric and AsLOV2 forms a monomer), might point toward a similar ("helix-out") orientation of the C-terminal extension in the two *Pseudomonas* LOV proteins and the truncated YtvA-LOV construct of the crystal structure. However, without further structural data, no unequivocal conclusions can be made as to the orientation both N- and C-terminal extensions as well as to the mode of dimerization.

Functional Significance and Phylogenetic Conservation of PpSB1-LOV- and PpSB2-LOV-like Proteins in Different Pseudomonas Strains. The lack of a fused effector domain in both *Pseudomonas* proteins suggests that protein−protein interactions must play a role in signaling by the two LOV proteins. The observation of a blue light effect in *P. putida*, such that selectively blue light irradiation results in an increased excretion of the iron scavenger pyoverdine under iron-limiting conditions (Krauss, Ph.D. Thesis, 2008), suggests that either PpSB1-LOV and/or PpSB2-LOV, as the only blue light receptors in the completely sequenced *P. putida* genome, could be involved in this physiological response. The presence of two highly similar LOV proteins with very different kinetic properties in the same organism raises the question whether these differences bear any functional importance or, more generally, whether the velocity of the dark recovery influences the biological sensor function of these LOV proteins. In such case, evolution should have retained those different velocities over time, and certain functional classes of LOV photoreceptors should show similar dark recovery kinetics. A recent review revealed that about 13% of the up to now identified bacterial LOV proteins are so-called "short" LOV's lacking a fused effector domain (*4*) but probably contain N- and C-terminal extensions of varying length. Thus, the two LOV proteins of *P. putida* KT2440 constitute the first two characterized examples of a structurally conserved family of bacterial LOV proteins whose biological function(s) remain(s) yet elusive. This family is largely restricted to proteobacterial lineages with members present in different Pseudomonads as well as in a few phototrophic α-Proteobacteria such as *Rhodobacter sphaeroides* (*4*). In several *Pseudomonas* strains like *P. putida* F1, *P. putida* W619, and *P. putida* KT2440, from which the two LOV proteins of this study have been cloned, invariably two "short" LOV proteins are present. A phylogenetic tree generated for several "short" *Pseudomonas* LOV proteins supports a classification into PpSB1-LOV and PpSB2-LOV-like clades (see Supporting Information Figure 4) and thus highlights the possibility of retaining fast (PpSB2-LOV) and slow reverting (PpSB1-LOV) proteins in one organism at a time. Moreover, in all LOV proteins affiliated with the PpSB1-LOV- like clade, invariably an arginine is present in the position corresponding to R66 in PpSB1-LOV. *Vice versa*, all proteins of the PpSB2-LOV-like clade possess an isoleucine corresponding to I66 in PpSB2-LOV (alignment not shown). This observation points toward an evolutionary (and maybe functional) conservation of LOV photochemical properties and implies the conservation of slow (PpSB1-LOV-like) and fast (PpSB2-LOV-like) recovering sensor proteins within one organism. Physiological studies currently underway in our laboratory will provide insights into this peculiar genetic feature of the genus *P. putida*.

CONCLUSIONS

Our study, performed on two highly similar bacterial LOV proteins, highlights the importance of residues in the FMN-binding pocket that form an intricate network to tune the dark recovery in LOV proteins. This effect can be drastic, since apparently a single mutation, namely, R66I in PpSB1-LOV, is sufficient to accelerate the dark recovery process by 2 orders of magnitude. The opposite mutation in PpSB2-LOV decelerates the kinetics significantly. Thus, our study indicates that strain, presumably imposed on the chromophore in the adduct state, effectively tunes the dark recovery in LOV proteins. Most importantly, stabilization versus destabilization of the adduct state seems to occur from amino acids surrounding the FMN phosphate. This mechanism, albeit realized differently in different proteins, might well represent a general mechanism for tuning the dark recovery in all LOV domain systems. An additional kinetic effect driven from surface-exposed histidine residues, suggested to be in place in plant LOV domains, cannot be ruled out to influence the dark recovery. However, based on our mutational analysis, this effect should be much less efficient as compared to tuning of the dark recovery caused by the R66−FMN phosphate interaction. While this report was under revision, a comprehensive study identified additional amino acid positions that effectively tune the dark recovery in different plant and bacterial LOV systems (*55*). Although the identified residues and the observed kinetic effects are different from those described here, the study further highlights the importance of the intricate network of amino acids surrounding the FMN chromophore that effectively tunes the dark recovery in LOV domains. CD experimental data led us to conclude that N- and C-terminal extensions to the LOV core in the two *Pseudomonas* proteins are at least partially helical. The absence of significant light-dependent secondary structural changes, mainly the absence of the loss of helical content, highlights the hypothesis that the signal-propagation mechanisms might not be conserved between plant and bacterial LOV systems. Nevertheless, conserved structural elements like the C-terminal (Jα) helical extensions could play a role in the signal propagation from the flavin chromophore in LOV domains to fused or interacting effector domains via LOV-associated structural elements.

ACKNOWLEDGMENT

The authors thank Björn Zorn (Max-Planck-Institute for Bioinorganic Chemistry, Muelheim an der Ruhr, Germany) for laser flash photolysis measurements.

SUPPORTING INFORMATION AVAILABLE

Table 1, oligonucleotides used throughout this study; Figure 1, multiple sequence alignment of LOV domains aiding mutation selection; Figure 2, UV/vis spectra of mutant LOV proteins; Figure 3, CD spectra of mutant LOV proteins; Figure 4, phylogenetic tree generated for selected *Pseudomonas* "short" LOV proteins; Figure 5, Jα helix orientations observed in

bacterial and plant LOV domain structures; Figure 6, laser flash photolysis measurements on PpSB1-LOV and PpSB2-LOV. This material is available free of charge via the Internet at http://pubs.acs.org.

REFERENCES

1. Christie, J. M., Salomon, M., Nozue, K., Wada, M., and Briggs, W. R. (1999) LOV (light, oxygen, or voltage) domains of the blue-light photoreceptor phototropin (nph1): binding sites for the chromophore flavin mononucleotide. *Proc. Natl. Acad. Sci. U.S.A. 96*, 8779–8783.
2. Briggs, W. R., and Christie, J. M. (2002) Phototropins 1 and 2: versatile plant blue-light receptors. *Trends Plant Sci. 7*, 204–210.
3. Ohgishi, M., Saji, K., Okada, K., and Sakai, T. (2004) Functional analysis of each blue light receptor, cry1, cry2, phot1, and phot2, by using combinatorial multiple mutants in *Arabidopsis*. *Proc. Natl. Acad. Sci. U.S.A. 101*, 2223–2228.
4. Losi, A., and Gärtner, W. (2008) Bacterial bilin- and flavin-binding photoreceptors. *Photochem. Photobiol. Sci. 7*, 1168–1178.
5. Losi, A., Polverini, E., Quest, B., and Gärtner, W. (2002) First evidence for phototropin-related blue-light receptors in prokaryotes. *Biophys. J. 82*, 2627–2634.
6. Krauss, U., Losi, A., Gärtner, W., Jaeger, K. E., and Eggert, T. (2005) Initial characterization of a blue-light sensing, phototropin-related protein from *Pseudomonas putida*: a paradigm for an extended LOV construct. *Phys. Chem. Chem. Phys. 7*, 2804–2811.
7. Losi, A. (2006) Flavin-based photoreceptors in bacteria, in Flavins: Photochemistry and Photobiology (Silva, E., and Edwards, A. M., Eds.) The Royal Society of Chemistry, Cambridge, U.K.
8. Avila-Perez, M., Hellingwerf, K. J., and Kort, R. (2006) Blue light activates the sigmaB-dependent stress response of *Bacillus subtilis* via YtvA. *J. Bacteriol. 188*, 6411–6414.
9. Purcell, E. B., Siegal-Gaskins, D., Rawling, D. C., Fiebig, A., and Crosson, S. (2007) A photosensory two-component system regulates bacterial cell attachment. *Proc. Natl. Acad. Sci. U.S.A. 104*, 18241–18246.
10. Swartz, T. E., Tseng, T. S., Frederickson, M. A., Paris, G., Comerci, D. J., Rajashekara, G., Kim, J. G., Mudgett, M. B., Splitter, G. A., Ugalde, R. A., Goldbaum, F. A., Briggs, W. R., and Bogomolni, R. A. (2007) Blue-light-activated histidine kinases: two-component sensors in bacteria. *Science 317*, 1090–1093.
11. Kennis, J. T., Crosson, S., Gauden, M., van Stokkum, I. H., Moffat, K., and van Grondelle, R. (2003) Primary reactions of the LOV2 domain of phototropin, a plant blue-light photoreceptor. *Biochemistry 42*, 3385–3392.
12. Kottke, T., Heberle, J., Hehn, D., Dick, B., and Hegemann, P. (2003) Phot-LOV1: photocycle of a blue-light receptor domain from the green alga *Chlamydomonas reinhardtii*. *Biophys. J. 84*, 1192–1201.
13. Swartz, T. E., Corchnoy, S. B., Christie, J. M., Lewis, J. W., Szundi, I., Briggs, W. R., and Bogomolni, R. A. (2001) The photocycle of a flavin-binding domain of the blue light photoreceptor phototropin. *J. Biol. Chem. 276*, 36493–36500.
14. Pfeifer, A., Majerus, T., Zikihara, K., Matsuoka, D., Tokutomi, S., Heberle, J., and Kottke, T. (2009) Time-resolved Fourier transform infrared study on photoadduct formation and secondary structural changes within the phototropin LOV domain. *Biophys. J. 96*, 1462–1470.
15. Kennis, J. T. M., and Akexandre, M. T. A. (2006) Mechanisms of light activation in flavin-binding photoreceptors, in Flavins: Photochemistry and Photobiology (Silva, E., and Edwards, A. M., Eds.) pp 287−319, Royal Society for Chemistry, Cambridge, U.K.
16. Alexandre, M. T., Domratcheva, T., Bonetti, C., van Wilderen, L. J., van Grondelle, R., Groot, M. L., Hellingwerf, K. J., and Kennis, J. T. (2009) Primary reactions of the LOV2 domain of phototropin studied with ultrafast mid-infrared spectroscopy and quantum chemistry. *Biophys. J. 97*, 227–237.
17. Pfeifer, A., Majerus, T., Zikihara, K., Matsuoka, D., Tokutomi, S., Heberle, J., and Kottke, T. (2009) Time-resolved Fourier transform infrared study on photoadduct formation and secondary structural changes within the phototropin LOV domain. *Biophys. J. 96*, 1462–1470.
18. Neiss, C., and Saalfrank, P. (2007) Ab initio quantum chemical investigation of the first steps of the photocycle of phototropin: a model study. *Photochem. Photobiol. 77*, 101–109.
19. Domratcheva, T., Fedorov, R., and Schlichting, I. (2006) Analysis of the primary photocycle reactions occurring in the light-oxygen-voltage blue-light receptor by multiconfigurational quantum-chemical methods. *J. Chem. Theory Comput. 2*, 1565–1574.
20. Losi, A. (2004) The bacterial counterparts of plants phototropins. *Photochem. Photobiol. Sci. 3*, 566–574.
21. Zikihara, K., Iwata, T., Matsuoka, D., Kandori, H., Todo, T., and Tokutomi, S. (2006) Photoreaction cycle of the light, oxygen, and voltage domain in FKF1 determined by low-temperature absorption spectroscopy. *Biochemistry 45*, 10828–10837.
22. Zoltowski, B. D., Schwerdtfeger, C., Widom, J., Loros, J. J., Bilwes, A. M., Dunlap, J. C., and Crane, B. R. (2007) Conformational switching in the fungal light sensor Vivid. *Science 316*, 1054–1057.
23. Crosson, S., and Moffat, K. (2001) Structure of a flavin-binding plant photoreceptor domain: insights into light-mediated signal transduction. *Proc. Natl. Acad. Sci. U.S.A. 98*, 2995–3000.
24. Fedorov, R., Schlichting, I., Hartmann, E., Domratcheva, T., Fuhrmann, M., and Hegemann, P. (2003) Crystal structures and molecular mechanism of a light-induced signaling switch: the Phot-LOV1 domain from *Chlamydomonas reinhardtii*. *Biophys. J. 84*, 2474–2482.
25. Alexandre, M. T., Arents, J. C., van Grondelle, R., Hellingwerf, K. J., and Kennis, J. T. (2007) A base-catalyzed mechanism for dark state recovery in the *Avena sativa* phototropin-1 LOV2 domain. *Biochemistry 46*, 3129–3137.
26. Christie, J. M., Corchnoy, S. B., Swartz, T. E., Hokenson, M., Han, I. S., Briggs, W. R., and Bogomolni, R. A. (2007) Steric interactions stabilize the signaling state of the LOV2 domain of phototropin 1. *Biochemistry 46*, 9310–9319.
27. Guo, H., Kottke, T., Hegemann, P., and Dick, B. (2005) The phot LOV2 domain and its interaction with LOV1. *Biophys. J. 89*, 402–412.
28. Studier, F. W. (2005) Protein production by auto-induction in high density shaking cultures. *Protein Expression Purif. 41*, 207–234.
29. Sambrook, J., and Russell, D. (2001) Molecular cloning: a laboratory manual, 3rd ed., Cold Spring Harbor Laboratory Press, Cold Spring Harbor, NY.
30. Buttani, V., Losi, A., Eggert, T., Krauss, U., Jaeger, K. E., Cao, Z., and Gärtner, W. (2007) Conformational analysis of the blue-light sensing protein YtvA reveals a competitive interface for LOV-LOV dimerization and interdomain interactions. *Photochem. Photobiol. Sci. 6*, 41–49.
31. Whitmore, L., and Wallace, B. A. (2004) DICHROWEB, an online server for protein secondary structure analyses from circular dichroism spectroscopic data. *Nucleic Acids Res. 32*, W668–W673.
32. Cao, Z., Buttani, V., Losi, A., and Gärtner, W. (2007) A blue light inducible two component signal transduction system in the plant pathogen *Pseudomonas syringae* pv. tomato. *Biophys. J. 94*, 897–905.
33. Schuler, L. D., Daura, X., and Van Gunsteren, W. F. (2001) An improved GROMOS96 force field for aliphatic hydrocarbons in the condensed phase. *J. Comput. Chem. 22*, 1205–1218.
34. Guex, N., and Peitsch, M. C. (1997) SWISS-MODEL and the Swiss-PdbViewer: an environment for comparative protein modeling. *Electrophoresis 18*, 2714–2723.
35. Gerber, P. R., and Muller, K. (1995) Mab, a generally applicable molecular-force field for structure modeling in medicinal chemistry. *J. Comput.-Aided Mol. Des. 9*, 251–268.
36. Emsley, P., and Cowtan, K. (2004) Coot: model-building tools for molecular graphics. *Acta Crystallogr. D 60*, 2126–2132.
37. Nicholas, K., Nicholas, H. J., and Deerfield, D. (1997) GeneDoc: analysis and visualization of genetic variation. *EMBNEWS 4*, 14.
38. Guindon, S., Lethiec, F., Duroux, P., and Gascuel, O. (2005) PHYML Online—a web server for fast maximum likelihood-based phylogenetic inference. *Nucleic Acids Res. 33*, W557–W559.
39. Keane, T. M., Naughton, T. J., and McInerney, J. O. (2007) MultiPhyl: a high-throughput phylogenomics webserver using distributed computing. *Nucleic Acids Res. 35*, W33–37.
40. Vinh le, S., and von Haeseler, A. (2004) IQPNNI: moving fast through tree space and stopping in time. *Mol. Biol. Evol. 21*, 1565–1571.
41. Drummond, A. J., and Rambaut, A. (2006) BEAST v1.4 , available from http://beast.bio.ed.ac.uk/.
42. Losi, A., Quest, B., and Gärtner, W. (2003) Listening to the blue: the time-resolved thermodynamics of the bacterial blue-light receptor YtvA and its isolated LOV domain. *Photochem. Photobiol. Sci. 2*, 759–766.
43. Losi, A., Ghiraldelli, E., Jansen, S., and Gärtner, W. (2005) Mutational effects on protein structural changes and interdomain interactions in the blue-light sensing LOV protein YtvA. *Photochem. Photobiol. 81*, 1145–1152.
44. Losi, A., Kottke, T., and Hegemann, P. (2004) Recording of blue light-induced energy and volume changes within the wild-type and mutated phot-LOV1 domain from *Chlamydomonas reinhardtii*. *Biophys. J. 86*, 1051–1060.

45. Fasman, G. D. (1996) Circular dichroism and the conformational analysis of biomolecules, Plenum Press, New York, NY.
46. Katsura, H., Zikihara, K., Okajima, K., Yoshihara, S., and Tokutomi, S. (2009) Oligomeric structure of LOV domains in *Arabidopsis* phototropin. *FEBS Lett. 583*, 526–530.
47. Nash, A. I., Ko, W. H., Harper, S. M., and Gardner, K. H. (2008) A conserved glutamine plays a central role in LOV domain signal transmission and its duration. *Biochemistry 47*, 13842–13849.
48. Corchnoy, S. B., Swartz, T. E., Lewis, J. W., Szundi, I., Briggs, W. R., and Bogomolni, R. A. (2003) Intramolecular proton transfers and structural changes during the photocycle of the LOV2 domain of phototropin 1. *J. Biol. Chem. 278*, 724–731.
49. Harper, S. M., Christie, J. M., and Gardner, K. H. (2004) Disruption of the LOV-Jalpha helix interaction activates phototropin kinase activity. *Biochemistry 43*, 16184–16192.
50. Harper, S. M., Neil, L. C., and Gardner, K. H. (2003) Structural basis of a phototropin light switch. *Science 301*, 1541–1544.
51. Yao, X., Rosen, M. K., and Gardner, K. H. (2008) Estimation of the available free energy in a LOV2-J alpha photoswitch. *Nat. Chem. Biol. 4*, 491–497.
52. Nakasone, Y., Eitoku, T., Matsuoka, D., Tokutomi, S., and Terazima, M. (2007) Dynamics of conformational changes of *Arabidopsis* phototropin 1 LOV2 with the linker domain. *J. Mol. Biol. 367*, 432–442.
53. Möglich, A., and Moffat, K. (2007) Structural basis for light-dependent signaling in the dimeric LOV domain of the photosensor YtvA. *J. Mol. Biol. 373*, 112–126.
54. Halavaty, A. S., and Moffat, K. (2007) N- and C-terminal flanking regions modulate light-induced signal transduction in the LOV2 domain of the blue light sensor phototropin 1 from *Avena sativa*. *Biochemistry 46*, 14001–14009.
55. Zoltowski, B. D., Vaccaro, B., and Crane, B. R. (2009) Mechanism-based tuning of a LOV domain photoreceptor, Nat. Chem. Biol. (Epub ahead of print doi:10.1038/nchembio.210).